This file is the final accepted version of the manuscript, published in
https://doi.org/10.1016/j.jobe.2023.108350

EXPERIMENTAL INVESTIGATION ON INFLUENCE OF TERRAIN COMPLEXITY FOR WIND PRESSURE OF LOW-RISE BUILDING

Lee-Sak An[1] and Sungmoon Jung[2]*

Abstract

This study conducted extensive wind tunnel tests to evaluate the impact of terrain complexity on wind pressure across low-rise buildings. A series of wind tunnel tests was performed using 50 actual terrain morphologies in the US. The findings were compared with results obtained from testing on homogeneous terrain to discern variations in pressure coefficients. A notable increase in turbulence intensity was observed in complex heterogeneous terrains, even with similar effective roughness lengths. The heightened turbulence property was a crucial factor in explaining changes in $C_{p,mean}$. The magnitude of $C_{p,mean}$ demonstrated a continuous rise in the windward wall and roof 1 regions with increasing turbulence intensity. This correlation held true even for $I_{u,eave}$ values surpassing 0.3. In contrast, while $C_{p,RMS}$ exhibited a tendency to increase with rising $I_{u,eave}$, it did not exhibit the same continuous increase phenomenon. Consequently, no significant disparity in magnitude was noted between homogeneous and heterogeneous terrains in this regard. These findings underscore the importance of accounting for terrain complexity in wind load assessments, particularly in scenarios of heightened terrain diversity, to mitigate potential errors in wind load evaluations.

Keywords

[1] Postdoctoral Scholar, Department of Civil and Environmental Engineering, FAMU-FSU College of Engineering, 2035 E Paul Dirac Dr, Tallahassee, Florida 32310, United States. Email: lan@eng.famu.fsu.edu

[2] Professor, Department of Civil and Environmental Engineering, FAMU-FSU College of Engineering, 2035 E Paul Dirac Dr, Tallahassee, Florida 32310, United States. Email: sjung@eng.famu.fsu.edu (corresponding author)

Wind tunnel testing; Real sites; Low-rise building; Pressure coefficient; Heterogeneous terrain; Terraformer

1. Introduction

Terrain configuration is a critical factor introducing uncertainties in wind loads, as underscored in Davenport's wind loading chain [1]. The influence of terrain roughness becomes particularly pronounced for low-rise buildings situated near the ground surface, as they are exposed to heightened turbulence. In practice, engineers often treat terrains with topological complexity as if they were homogeneous (uniform) terrains, categorized by 'exposure category'. This exposure-based approach has gained widespread acceptance [2]. However, some studies suggesting that upstream terrain configurations within a short distance upwind of a site have a direct impact on peak wind loads on building envelopes [3]. The effect of terrain complexity on wind load estimation remains insufficiently investigated.

Following Jensen's wind tunnel experiment, which established the similarity in using a turbulent boundary layer to obtain pressure coefficients in agreement with full-scale values [4], many full-scale and wind tunnel measurements have been conducted to assess wind loads on low-rise buildings. The focus has predominantly centered on urban or suburban exposures, emphasizing the impact on building structures. To avoid undersized low-rise building models that resemble matchboxes, when replicating the entire atmospheric boundary layer (ABL) in a wind tunnel, it is customary to simulate the lower portion commonly known as the atmospheric surface layer (ASL). This approach allows for the use of large-scale models for low-rise buildings, typically at a minimum scale of 1:50 [5]. The ASL is modelled based on roughness length (z_0) to simulate the underlying surface's influence on turbulent mixing. An effective roughness value for the entire

This file is the final accepted version of the manuscript, published in
https://doi.org/10.1016/j.jobe.2023.108350

area has been found to be sufficient in area with moderately homogeneous terrains and smaller-scale inhomogeneity (such as vegetation patches and built structures) [6, 7]. Regarding the concern over lower Reynolds numbers (*Re*) stemming from scaling effects in wind tunnel testing, there has been a consensus that *Re* can be relaxed at larger values above a certain threshold (i.e., $Re > 1.0 \times 10^5$) [2].

Ho et al. [8, 9] conducted wind tunnel tests on generic low-rise buildings for open and suburban exposures, observing higher wind loads in smoother terrains due to increased peak wind speeds. However, conversely, peak pressure coefficients can be higher in rougher terrains due to reduced mean wind speeds and increased turbulence intensity [10]. Wind tunnel tests under varying upstream exposure conditions were performed by Surry [11], Wang et al. [12], and Zisis and Stathopoulos [13], who compared their findings with field measurements. Fernandez-Caban and Masters [14] recently conducted extensive wind tunnel testing to probe the effects of upwind terrain on a generic low-rise structure using state-of-the-art facilities [15]. Moreover, contemporary researchers are increasingly exploring the application of machine learning techniques to predict the pressure coefficient of low-rise buildings [16, 17].

Despite such extensive studies, the majority of current knowledge is confined to homogeneous (i.e., uniform) terrain. However, terrains in the real world are often complex and have abrupt changes in surface roughness, and significant knowledge gaps remain regarding the influence of the complex heterogeneous terrain on the pressure experienced by low-rise buildings. very few studies have discussed the effect of terrain complexity on wind loads. Yu et al. [18] conducted wind tunnel tests using two real city terrain models and proposed a minimum upstream fetch length for wind tunnel testing. Wang and Stathopoulos [3] emphasized the significance of local, small-scale roughness changes in affecting the variation of the wind speed profile above heterogeneous terrain. Kim et al. [19] investigated the effect of a large group of surrounding buildings on a typical low-rise building by measuring wind pressure. They observed that, although the mean pressure coefficient decreased, the peak pressure coefficient could increase due to the enhancement of the turbulence component. An et al. [20] conducted extensive wind tunnel testing to explore wind characteristics over complex heterogeneous terrains. They quantified the relationship between the variance of geometric morphology and wind characteristics, ultimately concluding that terrain complexity significantly increased turbulence intensity levels. It is anticipated that pressure coefficients over complex heterogeneous terrains will differ from those over homogeneous terrains due to the substantial influence of turbulence properties in the approaching wind flow on the pressure field [21, 22].

This study systematically investigates the impact of complex heterogeneous terrain on wind loads for low-rise buildings. To achieve this, extensive wind tunnel testing was conducted using actual terrain morphologies from 50 locations in the US. The wind pressure data collected under homogeneous conditions served as the reference for comparison. By comparing the pressure coefficient of terrains with similar roughness lengths, we quantified the errors that may occur when ignoring terrain complexity and assuming a homogeneous terrain. Furthermore, through partitioning the building region, we individually assessed changes in pressure coefficients attributed to terrain complexity, identifying regions particularly susceptible to the effects of complex terrain.

The structure of this paper is as follows: Section 2 explains the testing setup, including overviews of the facility, the applied building model, and the site selection process. In Section 3, the roughness lengths of the selected terrains are determined through an anemometric approach, and subsequently the terrains are classified into exposure categories according to ASCE 7-22. Section

4 delves into the testing results, aiming to quantify the variability of pressure coefficients in complex heterogeneous terrain by comparing the experimental results with those from homogeneous terrains. Finally, we provide the conclusion in Section 5.

2. Test Setup

In this section, we provided a concise overview of the test setup, including an overview of the facility, the building model, and the site selection process. The DesignSafe-CI repository [23] offers comprehensive details about the test setup. For further details on the site selection and the reproduction of heterogeneous terrains from the real sites, refer to An et al. [20] and Alinejad et al. [24].

2.1. Wind Tunnel and Terraformer

The wind tunnel testing was carried out at the Natural Hazard Engineering Research Infrastructure (NHERI) experimental facility situated at the University of Florida [25]. Fig. 1 illustrates the schematic layout of the wind tunnel facility, which constitutes an open circuit tunnel with dimensions of 6 m (width) × 3 m (height) × 38 m (length). The tunnel inlet incorporates eight vane axial fans, each driven by a 56-kW electric motor. The flow generated by these fans conditioned by the multi-fan Flow Field Modulator (FFM) and honeycombs positioned approximately 3 m downwind from the fan bank.

This facility houses a fully automated terrain simulator named the "Terraformer." This state-of-the-art technology enables swift and precise terrain simulation, addressing the time-consuming and labor-intensive challenges associated with wind tunnel testing. The Terraformer consists of an array of 18 × 62 computer-controlled roughness blocks configured in a staggered layout, covering

This file is the final accepted version of the manuscript, published in
https://doi.org/10.1016/j.jobe.2023.108350

a fetch size of 6 m × 18.3 m. Each roughness element is equipped with an actuator, allowing for independent height adjustments. These elements possess a plan dimension of 100 mm × 50 mm and adjustable heights ranging from 0 to 160 mm. The element height is controlled through LabVIEW software, and the reconfiguration of all 1116 elements typically takes less than 60 s. Consequently, the Terraformer efficiently simulates an extensive series of homogeneous and heterogeneous upwind terrains. Additionally, a turntable located at the end of the upwind fetch enables the simulation of wind effects on structures at various wind incidence angles.

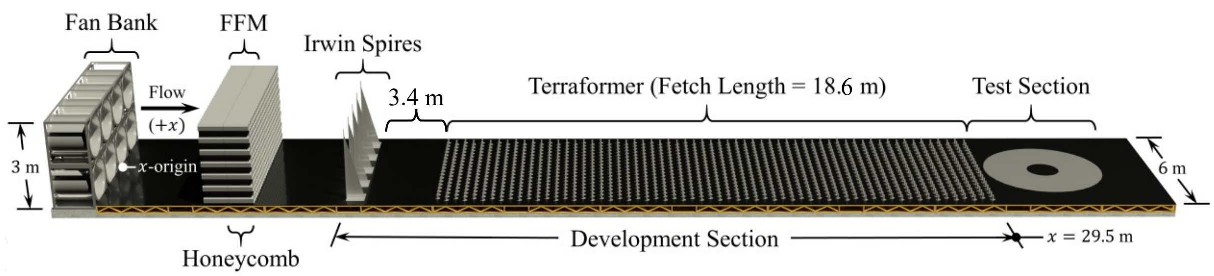

Fig. 1. Schematic plan of the wind tunnel facility at the University of Florida [26].

The wind speed was measured at a sampling rate of 1250 Hz using three Turbulent Flow Instrumentation Cobra probes positioned at the middle of the Terraformer's far end. To obtain the profile, wind speeds were measured at 36 different heights, ranging from 5 mm to 1500 mm above the ground. The wind profile was measured independently before placing the building model on the test section to mitigate the potential impact of the Cobra probe on the wind pressure.

To minimize adverse scale effects, model scales in wind tunnel testing are typically within the range of 1:10 to 1:100 [27]. In this study, we adopted a 1:50 scale, meaning the maximum vertical measurement height of 1500 mm in test scale corresponds to 75 m in full-scale representation. The speed scale is 3.5 ($\frac{V_{full}}{V_{test}} = \frac{35\ m/s}{10\ m/s}$; V_{full}=approximate hurricane condition in full scale [8]; V_{test}= the wind speed in the wind tunnel at 10 m height in full scale). The minimum test duration required for 10 minutes equivalent full-scale testing is 42 seconds. Wind speed measurements were taken over a period of 75 seconds.

2.2. Building Model

The low-rise building has dimensions of 274 mm × 182 mm × 80 mm in testing scale (13.7 m × 9.1 m × 4 m in full-scale) with a 1/4:12 gable roof slope, following the design of the Wind Engineering Research Field Laboratory (WERFL) building at Texas Tech University [11].

Pressure measurements were obtained using eight high-speed electronic scanning modules from Scanivalve ZOC33 [28]. Each module was housed within a robust thermal control unit made of stainless steel, equipped with an analog-to-digital module featuring remote Ethernet capability. The thermal control unit is operational in temperatures ranging from -45°C to 65°C. Pressure taps were connected to the modules via 122 cm long urethane tubing, and the sampling frequency was set at 625 Hz. Tubing effects on pressure measurements were adjusted to minimize distortion on amplitude and phase shift [29]. Pressure data were simultaneously recorded based on the time series. Fig. 2 provides a visual representation of the pressure tap layout on the building model. The building model was outfitted with a total of 216 pressure taps, comprising 102 roof taps and 114 wall taps. The tap positions adhered to the layout utilized in the WERFL model of the NIST aerodynamic database [8], with an additional 10 taps incorporated onto the roof to enhance spatial resolution.

Pressure on the low-rise building was examined using two distinct approaches: the tap line and roof contour. The tap line was aligned parallel to the X-axis, with the Y-coordinate set at 6.2 m in full-scale. This tap line has been consistently employed in previous studies to scrutinize flow separation and reattachment behavior on the building surfaces [8, 21]. Also, analyzing the roof pressure provides insight into the extent to which the suction on the roof fluctuates.

This file is the final accepted version of the manuscript, published in
https://doi.org/10.1016/j.jobe.2023.108350

The pressure coefficient at a point of interest, denoted as C_p, is defined as the ratio between the measured building surface gauge pressure and the roof-height dynamic pressure, expressed by the formula:

$$C_p(t) = \frac{p(t) - p_0}{0.5\rho U_H^2} \tag{1}$$

Here, U_H represents the wind speed at the eave height of the low-rise building (4 m), and ρ denotes the air density. The term $p(t) - p_0$ signifies the net wind pressure at the point of interest, with p_0 referring to the reference pressure.

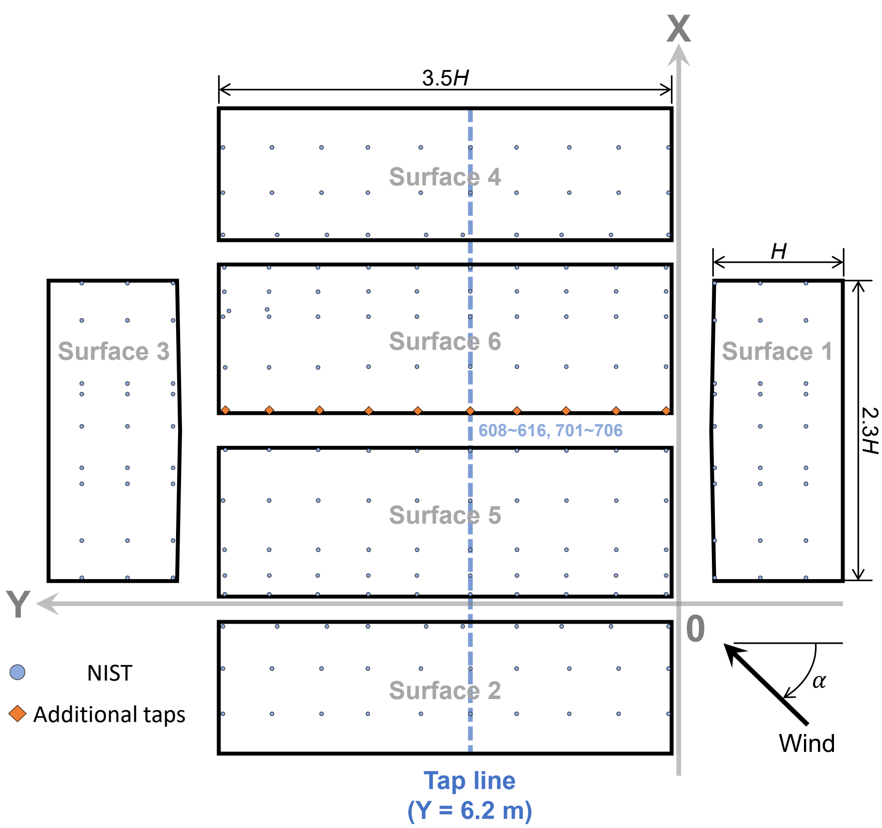

Fig. 2. Layout of pressure taps on the building models.

This file is the final accepted version of the manuscript, published in
https://doi.org/10.1016/j.jobe.2023.108350

2.3. Selection of Heterogeneous Terrains

Complex heterogeneous terrain configurations sourced from real terrains were compiled for wind tunnel testing. The primary data source was the National Land Cover Database (NLCD) [30] provided by the US Geological Survey. A total of 529 sites from 32 US states prone to hurricanes were selected. Each site image obtained from the NLCD dataset had dimensions of 3840 m × 3840 m. To create more comprehensive cases, each image was divided into four smaller images facing north, south, west, and east, with dimensions of 1860 m × 540 m each. This division resulted in a total of 2116 images for analysis.

The NLCD dataset furnished land coverage information for each pixel of the image, with a resolution of 30 m (each pixel covering 30 m × 30 m of land). By utilizing specific land coverage types and their corresponding local roughness length z_0^{local} values, as shown in Table 1, each pixel in the image was assigned an appropriate z_0^{local} value.

Table 1. Land coverage classification in NLCD images (z_0 range is based on Wieringa [7], Wang and Stathopoulos [3], Davenport [31], Vihma and Savijärvi [32], and He et al. [33])

Land cover	z_0^{local} (full-scale, m)	Block height (test-scale, m)
Open Water, Perennial Ice, Snow	0.0003	0.0060
Woody Wetlands, Emergent Herbaceous Wetland	0.0025	0.0100
Barren Land	0.0055	0.0125
Dwarf Scrub, Shrub Scrub	0.0105	0.0160
Pasture, Hay	0.0155	0.0180
Grassland, Herbaceous, Cultivated Corps	0.0205	0.0200
Low-rise building	0.5	0.0770
Mid- to high-rise	1	0.1110
Deciduous Forest, Evergreen Forest, Mixed Forest	1.65	0.1480

To select representative terrains with distinct stochastic properties of z_0^{local}, the k-means algorithm [34]—a commonly used clustering technique minimizing the average squared distance between points within the same cluster—was applied in the 2D space defined by the mean $\mu(z_0^{local})$ and standard deviation $\sigma(z_0^{local})$. This process led to the identification and classification of 50 distinct clusters.

This file is the final accepted version of the manuscript, published in
https://doi.org/10.1016/j.jobe.2023.108350

In the wind tunnel, these z_0^{local} values were correlated with the corresponding block heights using the improved Lettau relationship proposed by Macdonald et al. [35]. The block height information for each cover type is presented in Table 1. Fig. 3 provides examples of the selected sites and their corresponding block height maps in the Terraformer, along with the simulated terrain morphology generated for site 8.

Additionally, as reference cases for comparison with the complex heterogeneous terrains, preliminary wind tunnel testing was conducted for homogeneous terrains. All block heights (*H*) in the Terraformer were uniformly increased from 10 mm to 150 mm at 10 mm intervals.

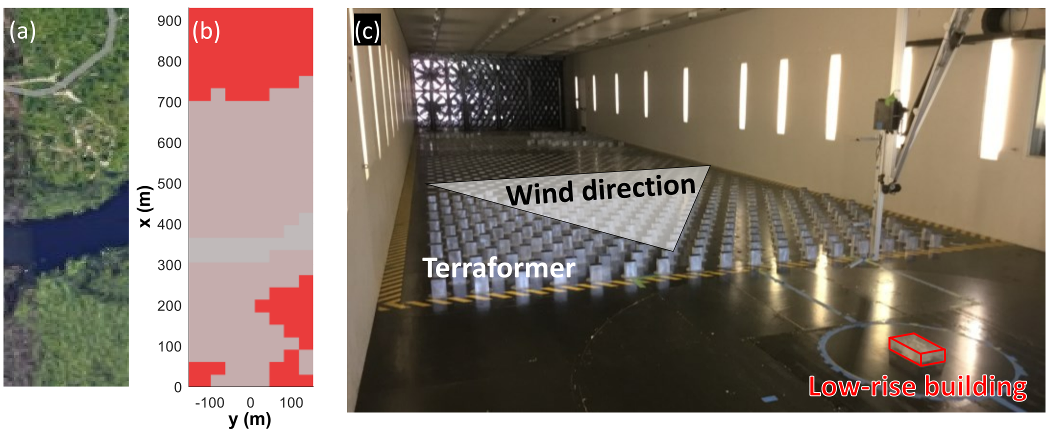

Fig. 3. Example of complex heterogeneous terrains (site 8): (a) Aerial view (Google Earth used for better visualization); (b) Block height map; and (c) Actual photo in the wind tunnel.

3. Wind Profiles and Exposure Categorization

The concept of the exposure categories is widely adopted into design standards globally, including the US [2], Canada [36], and Europe [37], to streamline the design process. In the US, ASCE 7-22 classifies terrain into one of three exposures: B to D, as outlined in Table 2 [2]. Each exposure category is defined based on the roughness length (z_0), which serves as a representative measure of the aerodynamic characteristics of the terrain. After categorizing both homogeneous

This file is the final accepted version of the manuscript, published in
https://doi.org/10.1016/j.jobe.2023.108350

and heterogeneous terrains by their exposure category, potential alterations arising from terrain heterogeneity within the same exposure category were meticulously quantified. It is noteworthy that Exposure A has been excluded since ASCE 7-02 due to the significant variability of wind in this terrain, arising from local channeling and wake-buffeting effects. Due to this uncertainty, sites identified with z_0 corresponding to Exposure A were excluded from subsequent analysis.

Table 2. Range of z_0 by exposure category [2] (adopted from ASCE 7-22 Table C26.7-1).

Exposure category	**Lower limit of z_0 (m)**	**Typical value of z_0 (m)**	**Upper limit of z_0 (m)**
A[a]	0.7	2	-
B[b]	0.15	0.3	0.7
C[c]	0.01	0.02	0.15
D[d]	-	0.005	0.01

[a]Centers of large cities (eliminated since ASCE 7-02)
[b]Urban and suburban terrain
[c]Open terrain
[d]Flat, unobstructed area and water surfaces

3.1. Calibration of ARPs

To determine the exposure category of the complex heterogeneous terrains, the effective roughness length ($z_{0,\text{eff}}$) for each terrain was obtained through anemometric approach [38, 39]. The curve fitting techniques are used to match the log law to velocity profiles measurements. Since wind profiles in lower atmospheric surface layer (ASL) are important for assessing low-rise buildings [40], we estimated aerodynamic roughness parameters (ARP), including friction velocity (u_*), zero-displacement height (d), and z_0, within inertial sublayer (ISL) [39]. The ISL nominally exists between $z_w < z < 0.25\delta$, where z_w is a wake diffusion height, where turbulent mixing sufficiently blends the individual element wakes to produce laterally homogeneous flow, and δ is a gradient height. z_w was assumed as the average height of the block elements in 1/3 of width direction × 1/6 of length direction (12 lines × 11 lines = 132 blocks) in the front of measurement points. δ was set as the maximum vertical height of the measurement (75 m in full-scale).

For verification of the calibrated $z_{0,\mathrm{eff}}$, the measured wind profiles were compared with the wind profile based on log law [41], which is widely recognized for its accuracy in representing the theoretical mean wind speed within the lower portion of the ABL [42].

$$U(z) = \frac{u_*}{\kappa} \ln \left(\frac{z-d}{z_0}\right) \tag{2}$$

$U(z)$ represents the mean along-wind speed at height z, and κ is von Karman's constant (=0.40). This equation holds when the surface is aerodynamically fully-rough, meaning that the surface-roughness Reynolds number $Re_* = u_* z_0/\nu > 2.5$ [43], where ν is the kinematic viscosity of air. All wind tunnel testing results for complex heterogeneous terrains showed Re_* values higher than 2.5. Fig. 4 showcases the measured and predicted wind profiles at sites 1, 5, 39 and 49. Both measured and predicted wind profiles were normalized by the U_{max} of the measured wind profile. The predicted wind profile aligns well with the measured wind profiles within the ISL range, indicating that the $z_{0,\mathrm{eff}}$ based on the anemometric approach accurately represents the wind profiles of the corresponding complex heterogeneous terrains.

This file is the final accepted version of the manuscript, published in
https://doi.org/10.1016/j.jobe.2023.108350

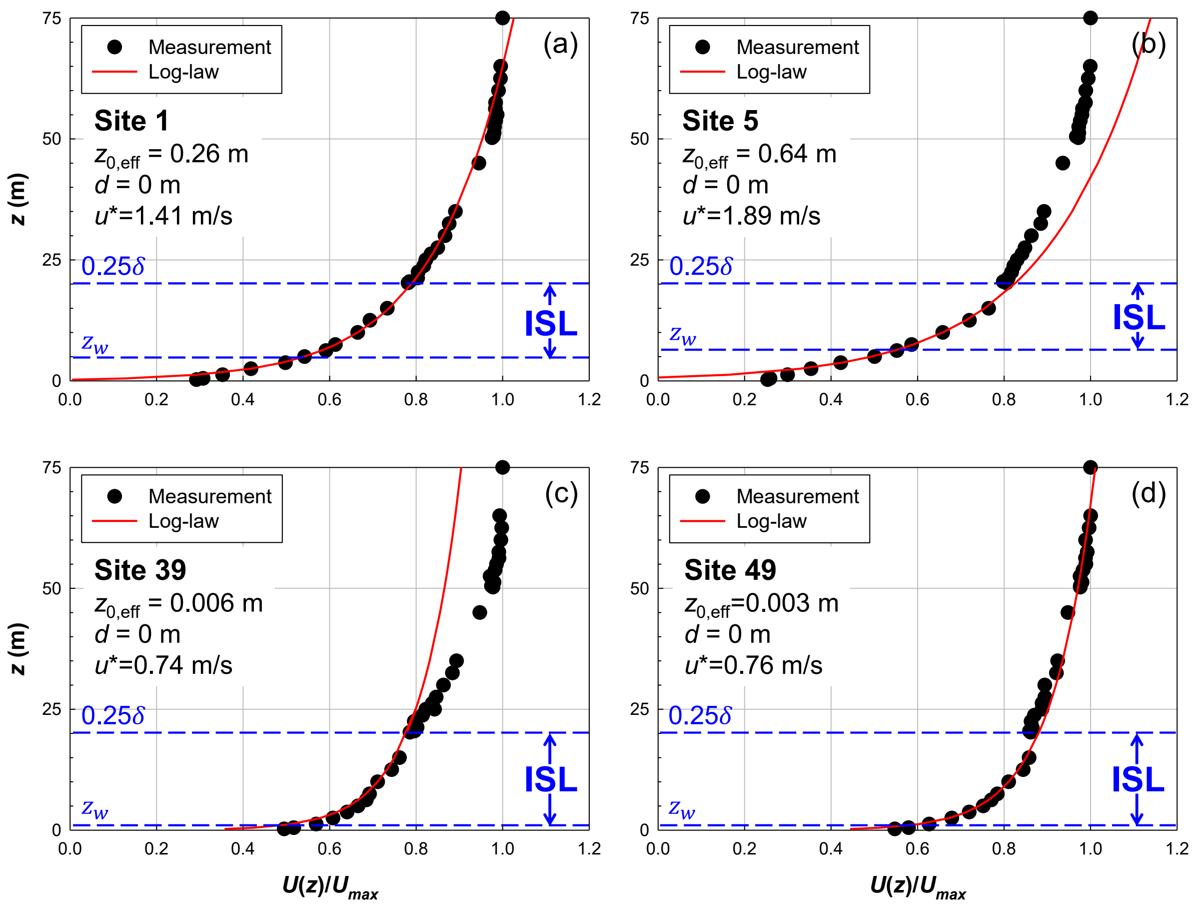

Fig. 4. Examples of the ARP calibration based on anemometric approach: (a) Site 1; (b) Site 5; (c) Site 39; and (d) Site 49.

3.2. Exposure Categorization

Tables 3 and 4 present the calculated $z_{0,\mathrm{eff}}$ values along with their corresponding exposure categories for both heterogeneous and homogeneous terrains. It is worth noting that Exposure B contains the highest number of sites (37 of 50 sites), which was possible to expect given that Exposure B encompasses a relatively wider range of z_0 values compared to Exposure C and D, making it the most common exposure category.

This file is the final accepted version of the manuscript, published in
https://doi.org/10.1016/j.jobe.2023.108350

Table 3. $z_{0,\mathrm{eff}}$ in full-scale and corresponding exposure categories for complex heterogeneous terrain.

Site	$z_{0,\mathrm{eff}}$ (m)	Exposure category	Site	$z_{0,\mathrm{eff}}$ (m)	Exposure category
34	0.002	D	24	0.342	B
49	0.003		23	0.343	
39	0.006		18	0.355	
12	0.008		14	0.355	
36	0.011	C	32	0.357	
45	0.017		22	0.362	
13	0.081		30	0.367	
27	0.215	B	9	0.368	
40	0.229		10	0.370	
16	0.236		15	0.373	
25	0.237		20	0.391	
1	0.264		28	0.392	
4	0.305		19	0.399	
42	0.306		26	0.402	
43	0.311		48	0.427	
3	0.320		21	0.505	
38	0.323		29	0.524	
41	0.323		11	0.604	
46	0.326		5	0.639	
44	0.329		37	0.782	A
47	0.330		50	0.904	
2	0.334		7	0.929	
17	0.339		31	0.942	
6	0.339		33	1.241	
35	0.339		8	1.289	

Table 4. $z_{0,\mathrm{eff}}$ in full-scale and corresponding exposure categories for homogeneous terrain.

H **(testing scale, m)**	$z_{0,\mathrm{eff}}$ (m)	Exposure category
0.01	0.001	D
0.02	0.01	C
0.03	0.04	
0.04	0.08	
0.05	0.12	
0.06	0.16	B
0.07	0.21	
0.08	0.26	
0.09	0.32	
0.10	0.38	
0.11	0.46	
0.12	0.53	
0.13	0.62	
0.14	0.72	A
0.15	0.83	

This file is the final accepted version of the manuscript, published in
https://doi.org/10.1016/j.jobe.2023.108350

3.3. Wind Characteristics

Fig. 5 displays the normalized mean wind speed (U_{eave}/U_{max}) and turbulence intensity ($I_{u,eave}$) measured at the eave height (4 m) over both complex heterogeneous and homogeneous terrains. While both terrain types exhibit a decaying exponential relationship between U_{eave}/U_{max} and $I_{u,eave}$, complex heterogeneous terrain shows approximately 35% higher $I_{u,eave}$ compared to homogeneous terrain at similar U_{eave}/U_{max} levels. In Exposures C and D, characterized by relatively smooth roughness lengths, the differences between homogeneous and heterogeneous terrains are modest, largely due to the lower $I_{u,eave}$ level. However, in Exposure B, the contrast becomes more pronounced due to the elevated $I_{u,eave}$.

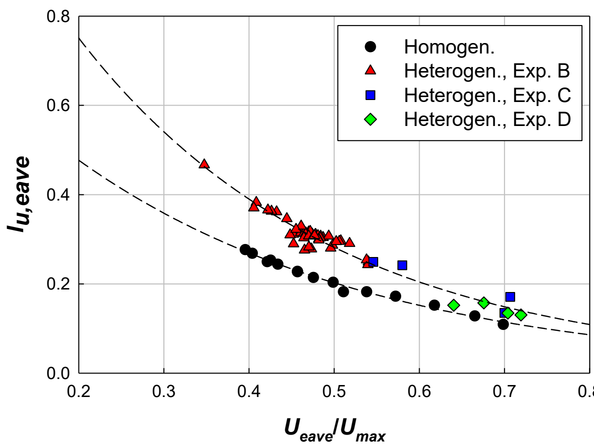

Fig. 5. Relationship between U_{eave}/U_{max} and $I_{u,eave}$ for heterogeneous and homogeneous terrains.

Fig. 6 depicts the altered wind characteristics attributed to the terrain complexity. Probability densities of U_{eave}/U_{max} and $I_{u,eave}$ are presented for Exposure B. As shown in Fig. 6 (a), the probability densities for heterogeneous terrains demonstrate similar mean and standard deviation values as those observed in homogeneous terrains. Consequently, the mean wind speed levels appear comparable between homogeneous and heterogeneous terrains. This result aligns with expectations, as exposure categories were classified based on $z_{0,\mathrm{eff}}$, determined through an anemometric approach utilizing the mean wind profile.

This file is the final accepted version of the manuscript, published in
https://doi.org/10.1016/j.jobe.2023.108350

However, in the case of $I_{u,eave}$ as depicted in Fig. 6 (b), both the mean and standard deviation exhibited an increase on complex heterogeneous terrain when compared to the homogeneous terrains. This observation, evident in Figs. 5 and 6, underscores how the terrain complexity of complex heterogeneous terrain enhances turbulence intensity even within the same exposure category. Given that turbulence properties in the approaching wind flow significantly impact the pressure distribution [21], such a discrepancy in $I_{u,eave}$ can lead to an unexpected variation in the pressure coefficient experienced by the low-rise building.

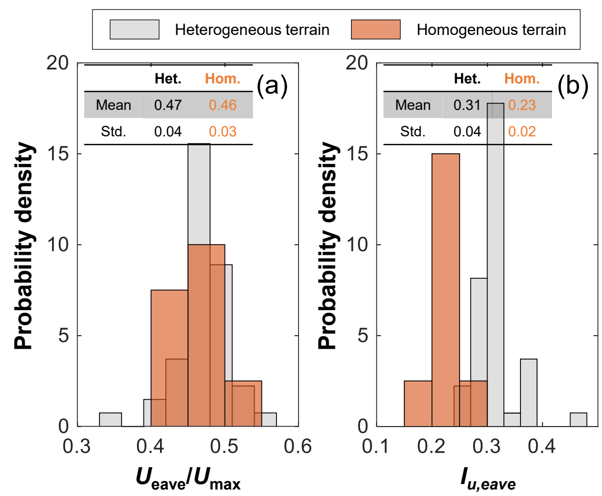

Fig. 6. Probability density of wind characteristics at eave height for Exposure B: (a) $U_{\mathrm{eave}}/U_{max}$; and (b) $I_{u,eave}$.

Ensuring similarity in the turbulence characteristics of the inflow wind is crucial for accurately predicting unsteady wind loads. Fig. 7 presents the wind power spectrum at eave heights for both complex heterogeneous and homogeneous terrains, featuring similar $z_{0,\mathrm{eff}}$ values (0.32 m). The power spectrum was determined through Fast Fourier Transform (FFT) using the Welch method [44]. The full-scale time series were segmented into 1-minute sub-segments with a 50% overlap. The Hamming window was applied to mitigate side-lobe leakage. Additionally, for comparison, the empirical model from the Engineering Sciences Data Unit (ESDU) [45], defined by Eq. (3), is included in the plots.

This file is the final accepted version of the manuscript, published in
https://doi.org/10.1016/j.jobe.2023.108350

$$\frac{nS_{uu}}{\sigma_u^2} = \frac{4f}{(1+70.8f^2)^{5/6}} \tag{3}$$

Here, S_{uu} denotes the power spectrum for the longitudinal turbulence component, n is the frequency (Hz), σ_u represents the standard deviation of the fluctuating wind components, and $f = nL_u^x/U$, where L_u^x stands for the longitudinal integral length scale, and U is the mean wind speed.

For both types of terrain, the measured spectrum closely corresponds with the ESDU empirical model. In the case of the heterogeneous site, there is notably more energy at higher frequencies compared to the homogeneous case. Moreover, the heterogeneous spectrum exhibits a greater overall variance, indicating higher turbulence levels.

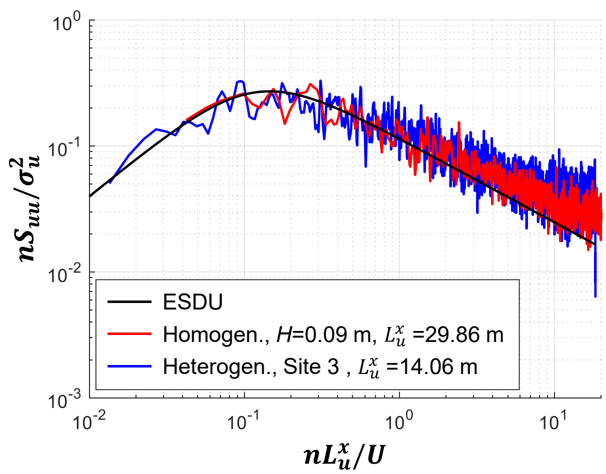

Fig. 7. Wind power spectrum at eave height for homogeneous terrain and complex heterogeneous terrain.

4. Results and Discussion

A comparative analysis of pressure coefficients between homogeneous and complex heterogeneous terrains was conducted. The investigation primarily focused on the mean ($C_{p,mean}$), root-mean-square ($C_{p,RMS}$), and peak ($C_{p,min}$ and $C_{p,max}$) pressure coefficients. The estimation of peak pressure coefficients was carried out using the Gumbel distribution fitting method, widely employed in practice [46]. Gumbel parameters were computed utilizing the Liblein BLUE formulation [47]. A total of 15 observed peaks were used for estimating the Gumbel parameters, aiming to obtain the best-expected peak for the entire record as reported by Gavanski et al. [46].

4.1. Tap Line

Fig. 8 illustrates the (i) $C_{p,mean}$, (j) $C_{p,\,RMS}$, and (k) $C_{p,min}$ at the tap line within Exposure B for three wind incidence angles: (a) 0°, (b) 45°, and (c) 90°. The statistics derived from complex heterogeneous terrains are presented as boxplots. Meanwhile, those obtained from homogeneous terrains are selectively shown for the lower bound (LB, $z_{0,\mathrm{eff}}$ = 0.16 m), typical value (TYP, $z_{0,\mathrm{eff}}$ = 0.30 m), and upper bound (UB, $z_{0,\mathrm{eff}}$ = 0.62 m) of Exposure B (Refer to Table 4). The tap line's position was normalized by the building height h (x/h=0 signifies the leading edge of the building).

On the roof region, the peaks of the three statistics were primarily located around the leading edge, within the range of $0<x/h<1$. While the trend of separated and reattached flow regions observed in complex heterogeneous terrains was consistent with that of the homogeneous terrain, the complex heterogeneous terrains exhibited a larger magnitude of the pressure coefficient than the homogeneous terrain in the separated region. Particularly, the amplification of the peak of $C_{p,mean}$ was noticeable at the windward wall and the roof. As shown in Fig. 8 (c-i), the peak of $C_{p,mean}$ on the roof at 90° occurred at x/h=0.36. In homogeneous terrain, the peak was approximately -1.2 and there was no significant change in the $C_{p,mean}$ level within Exposure B. However, in the heterogeneous terrain, it ranged between -1.2 and -2.0. The overall level and variability of $C_{p,mean}$ increased.

In the case of $C_{p,RMS}$, the difference trend between homogeneous and heterogeneous terrain differed slightly from $C_{p,mean}$. $C_{p,RMS}$ also demonstrated an increase in variability in complex heterogeneous terrains, but the overall level did not change as much as $C_{p,mean}$. At x/h = 0.36 in 45°

of wind incident angle (Fig. 8 (b-j)), $C_{p,RMS}$ in homogeneous terrain ranged between 0.52 and 0.64. Meanwhile, in the heterogeneous terrains, $C_{p,RMS}$ ranged from 0.57 to 0.87.

Regarding $C_{p,min}$, the peak range did not change significantly compared to $C_{p,mean}$ or $C_{p,RMS}$. Both terrains showed a consistent peak $C_{p,min}$ about -8 at around x/h=0.1~0.4. This observation indicated that the peak $C_{p,min}$ can take into account the effects of wind gusts and is insensitive to the upstream turbulence levels, which was consistent with the results reported by Wang et al. [12].

As shown in Fig. 8 (a), when the wind incident angle is 0°, there were no significant changes in statistics according to x/h because the direction of the tap line was perpendicular to the wind direction. Peaks occurred in the area close to the edges (around x/h = 0 and 2.3).

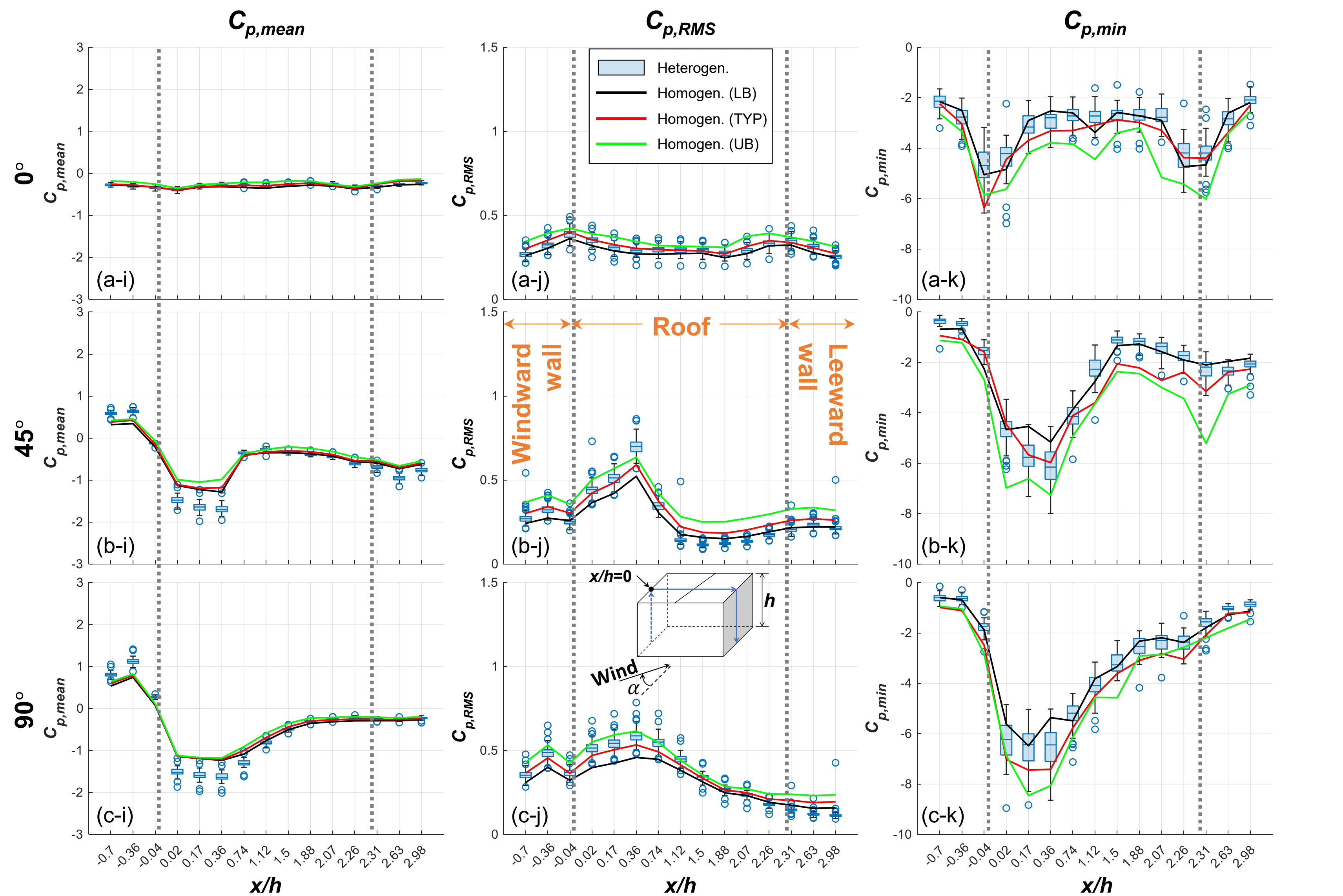

Fig. 8. Pressure coefficient statistics for homogeneous and heterogeneous terrains at the tap line, Exposure B: (a) 0°; (b) 45°; and (c) 90°; with (i) $C_{p,mean}$; (j) $C_{p,RMS}$; and (k) $C_{p,min}$.

For a more precise quantification of the differences in pressure coefficients, four peak statistics were extracted on the tap line for both complex heterogeneous and homogeneous cases: peak $C_{p,mean}$, maximum $C_{p,RMS}$, minimum $C_{p,min}$, and maximum $C_{p,max}$. Given the variation in pressure distribution across a low-rise building, we conducted individual investigations on the windward wall, roof, and leeward wall. To further distinguish between the upwind region, characterized by significant suction due to flow separation, and the downwind region, the roof was divided into two sections: Roof 1 ($0<x/h<1.8$) and Roof 2 ($1.8<x/h<2.3$). Note that the peak $C_{p,mean}$ corresponds to the maximum $C_{p,mean}$ on the windward wall, and the minimum $C_{p,mean}$ for other regions. Fig. 9 provides a visual representation of these peaks for each region with varying $z_{0,\mathrm{eff}}$ at a wind incidence angle of 90°. Fig. 9 (i) displays peak statistics across all homogeneous and heterogeneous terrains (the entire $z_{0,\mathrm{eff}}$ range). The y-axis range is unified from -15 to 10 for easy comparison of magnitudes across different regions. In wind tunnel testing, a z_0 of 0.3 m was commonly used for suburban terrains [8, 48, 49]. Fig. 9 (j) delves into the statistics of the pressure coefficient around the typical z_0 value for Exposure B (0.30 m$<z_{0,\mathrm{eff}}<$0.34 m), focusing on enlarged representations of enlarged $C_{p,mean}$, $C_{p,RMS}$, and the dominant peak pressure coefficients ($C_{p,max}$ in windward wall and $C_{p,min}$ in other regions). Additionally, Fig. 9 (k) provides a closer view of Fig. 9 (j), particularly zooming in on $C_{p,mean}$.

The peak of statistics exhibited an increase with rising $z_{0,\mathrm{eff}}$ values across all regions, irrespective of whether the terrain was homogeneous or complex heterogeneous. The fluctuations observed in pressures stemming from the oscillation and resizing of vortices are directly impacted by the turbulence of the wind [50, 51]. It was thus natural that the peaks of statistics would rise with increasing $z_{0,\mathrm{eff}}$. Notably, the results obtained from complex heterogeneous terrains revealed larger magnitudes or variability compared to their homogeneous counterparts, with the extent of the difference dependent on the specific statistic or geometric location.

As Fig. 9 (i) illustrates, higher magnitudes of $C_{p,mean}$, and peak C_p were evident on the windward wall and roof 1 when compared to roof 2 and the leeward wall. The windward wall experienced predominantly positive pressure since this region was directly exposed to the incoming wind flow. In roof 1, flow separation occurred, leading to strong negative pressure (i.e., suction) in this region. Roof 2 and the leeward wall, on the other hand, were affected by flow reattachment and the wake generated by the structure itself. This resulted in a more turbulent and unsteady flow, translating to lower wind pressures when compared to the windward wall and roof 1.

As shown in Fig. 9 (a-k) and (b-k), in the windward wall and roof 1, differences in the degree of $C_{p,mean}$ between homogeneous and complex heterogeneous terrains were apparent. In the windward wall, the maximum $C_{p,mean}$ ranged from 1.2 to 1.4 in the heterogeneous case, while it was approximately 0.8 in the homogeneous case. In roof 1, $C_{p,mean}$ in homogeneous terrain hovered around -1.0, whereas it approached -1.5 in heterogeneous terrain. Conversely, as demonstrated in Fig. 9 (a-j) and (b-j), no discernible difference in the overall level was observed for $C_{p,RMS}$ and the dominant peak C_p between homogeneous terrain and heterogeneous terrain. However, there was a clear increase in dispersion in the heterogeneous cases.

Fig. 9 (c) and (d) depict the peak of statistics on the roof 2 and the leeward wall. In these regions, changes attributed to terrain complexity were insignificant. There was scarcely any disparity in the levels between homogeneous and heterogeneous terrains for $C_{p,mean}$ and $C_{p,RMS}$. Although the variability of minimum $C_{p,min}$ increased in the heterogeneous case, the magnitude was quite small when compared to the windward or roof 1 regions. Hence, the absolute change remained modest.

This file is the final accepted version of the manuscript, published in
https://doi.org/10.1016/j.jobe.2023.108350

Consequently, $C_{p,mean}$ can be amplified by up to about 75% on the windward wall, and by about 50% on roof 1. In roof 2 and the leeward wall regions, the alteration in pressure coefficient due to terrain complexity was marginal.

This file is the final accepted version of the manuscript, published in
https://doi.org/10.1016/j.jobe.2023.108350

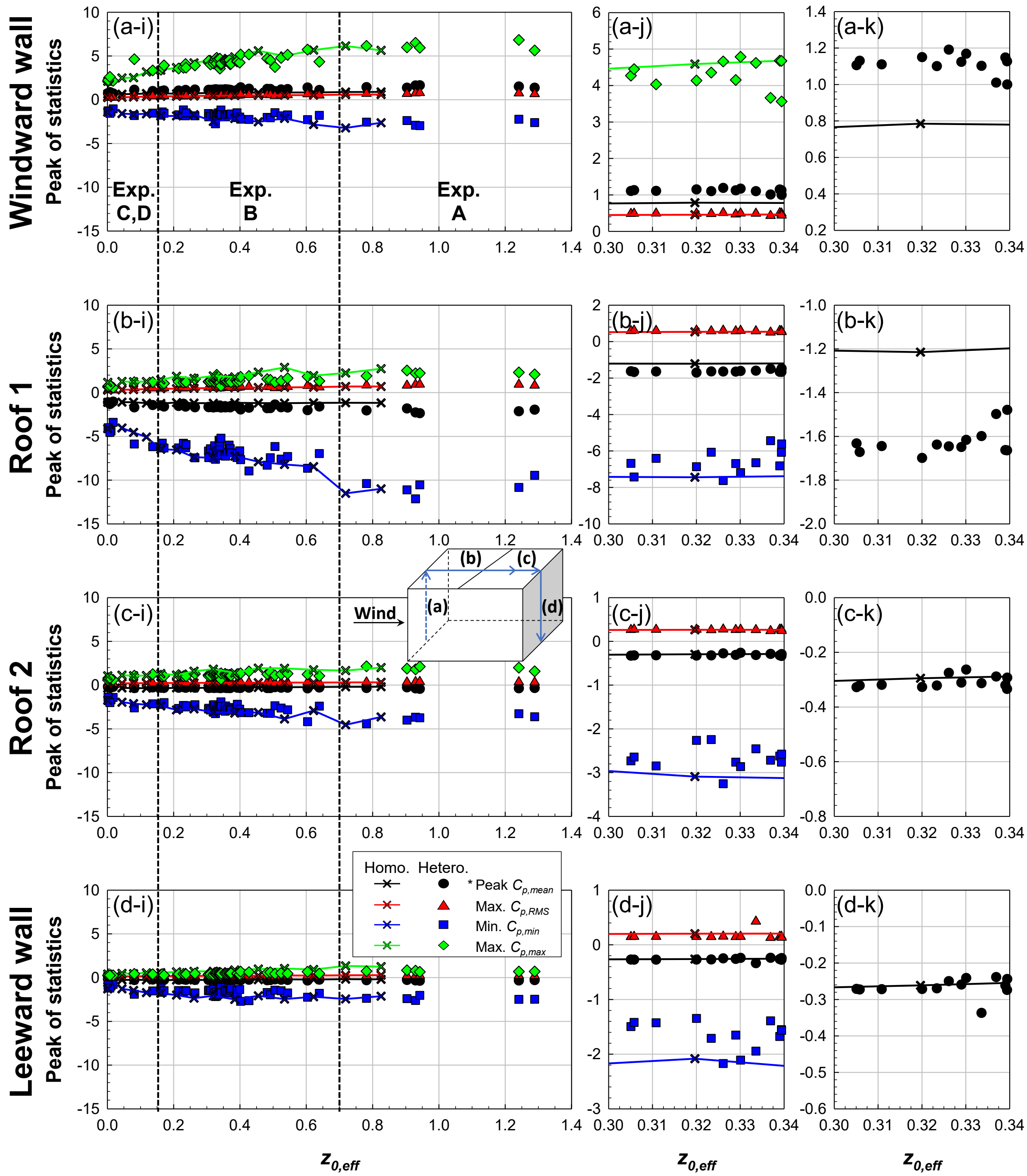

Fig. 9. Relationship between $z_{0,\mathrm{eff}}$ and peak statistics at the tap line for 90°: (a) Windward wall; (b) Roof 1; (c) Roof 2; and (d) Leeward wall; with (i) Full measured $z_{0,\mathrm{eff}}$ range; (j) $z_{0,\mathrm{eff}}$ range 0.30 to 0.34, and (k) Enlarged for peak $C_{p,mean}$. *Peak $C_{p,mean}$ indicates maximum $C_{p,mean}$ in the windward wall, and minimum $C_{p,mean}$ in the roof and leeward wall.

As observed in Figs. 8 and 9, the peak $C_{p,mean}$ can be amplified on heterogeneous terrain even when exposed to the same category of exposure and possessing similar $z_{0,\mathrm{eff}}$ values. These findings suggested that errors might arise in wind load assessments if real terrain complexities were oversimplified as homogeneous terrain during the design process. As we confirmed in Section 3.3, terrain complexity resulted in higher $I_{u,eave}$ values compared to homogeneous terrains in the same exposure categories. Elevated turbulence intensities play a pivotal role in reinforcing vortices within the separated shear layer, which in turn generates stronger pressure fluctuations [21, 52]. Thus, the increased magnitudes of $C_{p,mean}$ in complex heterogeneous terrains could be attributed to the turbulence properties of the wind flow.

The relationship between $I_{u,eave}$ and the peak $C_{p,mean}$ at a wind angle of 90° is depicted in Fig. 10. In the windward wall and roof 1, as shown in Fig. 10 (a) and (b), both the maximum and minimum $C_{p,mean}$ increased with higher $I_{u,eave}$ values. Particularly, in Fig. 10 (b), the results of Akon and Kopp [53], Okada and Ha [54], and Tieleman et al. [50] are presented alongside our observations. They also utilized the WERFL model and conducted wind tunnel tests simulating open and suburban terrains using homogeneous block arrays. In their testing, I_u ranged from 0.1 to 0.3, and the measured minimum $C_{p,mean}$ was comparable to the results from the homogeneous cases in this study.

For roof 2 and the leeward wall, as shown in Fig. 10 (c) and (d), no discernible relationship between minimum $C_{p,mean}$ and $I_{u,eave}$ was observed. Irrespective of of $I_{u,eave}$, values of -0.2 to -0.4 were observed in roof 2, while values of -0.15 to -0.35 were noted in the leeward wall. Combining the insights gained from Figs. 9 and 10, it could be concluded that the minimum $C_{p,mean}$ in roof 2 and leeward wall regions shows no correlation with turbulence properties resulting from terrain complexity. The change in minimum $C_{p,mean}$ in roof 2 and the leeward wall regions could be primarily explained to $z_{0,\mathrm{eff}}$.

The measured minimum $C_{p,mean}$ exhibited a relatively larger magnitude compared to previous studies involving low-rise buildings [8, 12, 53]. The key difference between this study and earlier ones lies in the level of turbulence intensity. In homogeneous conditions, it was rare to observe $I_{u,eave}$ values exceeding 0.3, as seen in this test and in numerous prior wind tunnel experiments [8, 12, 53]. However, in complex heterogeneous terrains, $I_{u,eave}$ can attain higher levels. It has been firmly established in previous studies that $C_{p,mean}$ increases with rise of $I_{u,eave}$. $C_{p,mean}$ was observed to exhibit a continuous increase even in cases where $I_{u,eave}$ exceeded 0.3.

Fig. 11 presents the maximum $C_{p,RMS}$. The peak magnitude of $C_{p,RMS}$ increased as $I_{u,eave}$ rose in both homogeneous and heterogeneous terrain. This trend was similarly observed in a previous study by Fernández-Cabán and Masters [55], which conducted a series of wind tunnel tests for homogeneous terrains with increasing block height. However, in complex heterogeneous terrains, the increase in $C_{p,RMS}$ did not continue as $I_{u,eave}$ increases, unlike $C_{p,mean}$. Although heterogeneous terrain exhibited higher $I_{u,eave}$, it shows similar levels of $C_{p,RMS}$ as homogeneous terrain. As a result, as seen in Fig. 9, the overall magnitudes of $C_{p,RMS}$ were similar between homogeneous terrain and complex heterogeneous terrain, but the dispersion increases at the complex heterogeneous terrain.

This file is the final accepted version of the manuscript, published in
https://doi.org/10.1016/j.jobe.2023.108350

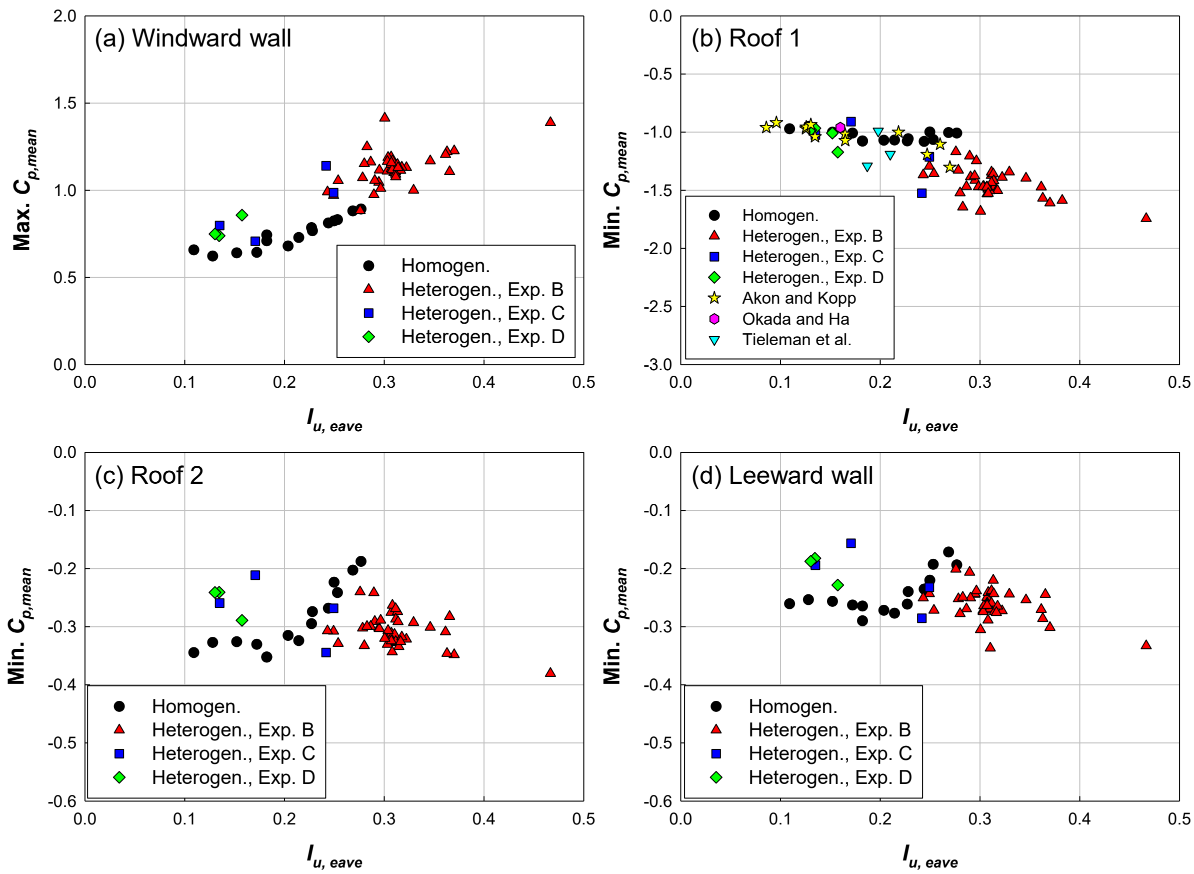

420 Fig. 10. Relationship between $I_{u,eave}$ and the peak $C_{p,mean}$ at a wind angle of 90°: (a) Windward wall; (b) Roof 1; (c)
421 Roof 2; and (d) Leeward wall.

422

This file is the final accepted version of the manuscript, published in
https://doi.org/10.1016/j.jobe.2023.108350

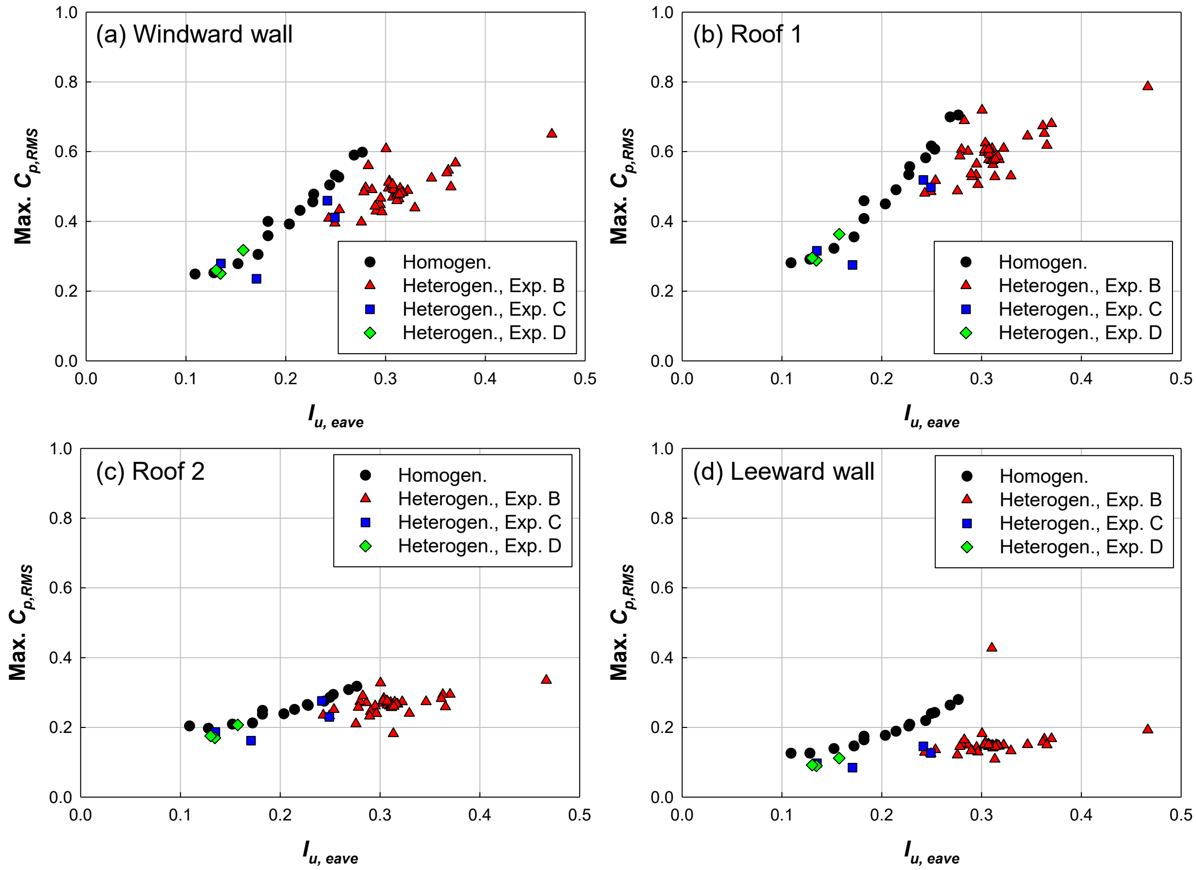

Fig. 11. Relationship between $I_{u,eave}$ and the maximum $C_{p,RMS}$ at a wind angle of 90°: (a) Windward wall; (b) Roof 1; (c) Roof 2; and (d) Leeward wall.

4.2. Roof Contour

Roof contours were compared to examine how the terrain complexity influence the pressure coefficient on the building roof when $z_{0,\mathrm{eff}}$ is similar. Figs. 12 and 13 present the roof contours of $C_{p,mean}$ and $C_{p,RMS}$, respectively. In both figures, (a) homogeneous terrain (H=0.09 m, $z_{0,\mathrm{eff}}$ = 0.32 m) and (b) complex heterogeneous terrain (0.30 m<$z_{0,\mathrm{eff}}$<0.34 m) are compared along with the three wind incident angles: (i) 0°, (j) 45°, and (k) 90°. In the case of heterogeneous terrains, the roof contours display the peak values for each tap among the selected sites (i.e., envelope). To maintain consistency in contour color, the color bar range has been standardized for each angle.

This file is the final accepted version of the manuscript, published in
https://doi.org/10.1016/j.jobe.2023.108350

In $C_{p,mean}$, the largest magnitude occurred near the corner of leading edge for both terrains. The heterogeneous terrain exhibited a larger magnitude, and it also demonstrated a longer reattachment length. This was because as longitudinal turbulence intensity increases, the mixing in the shear layers enhance the rate of entrainment, which reduces the shear layer's radius of curvature [55, 56].

The largest $C_{p,\ RMS}$ also occurred near the corner of the leading edge, and there was no significant difference in its magnitude level between homogeneous and heterogeneous. This result was similar result to what observed in the roof 1 and 2 regions of the tap line.

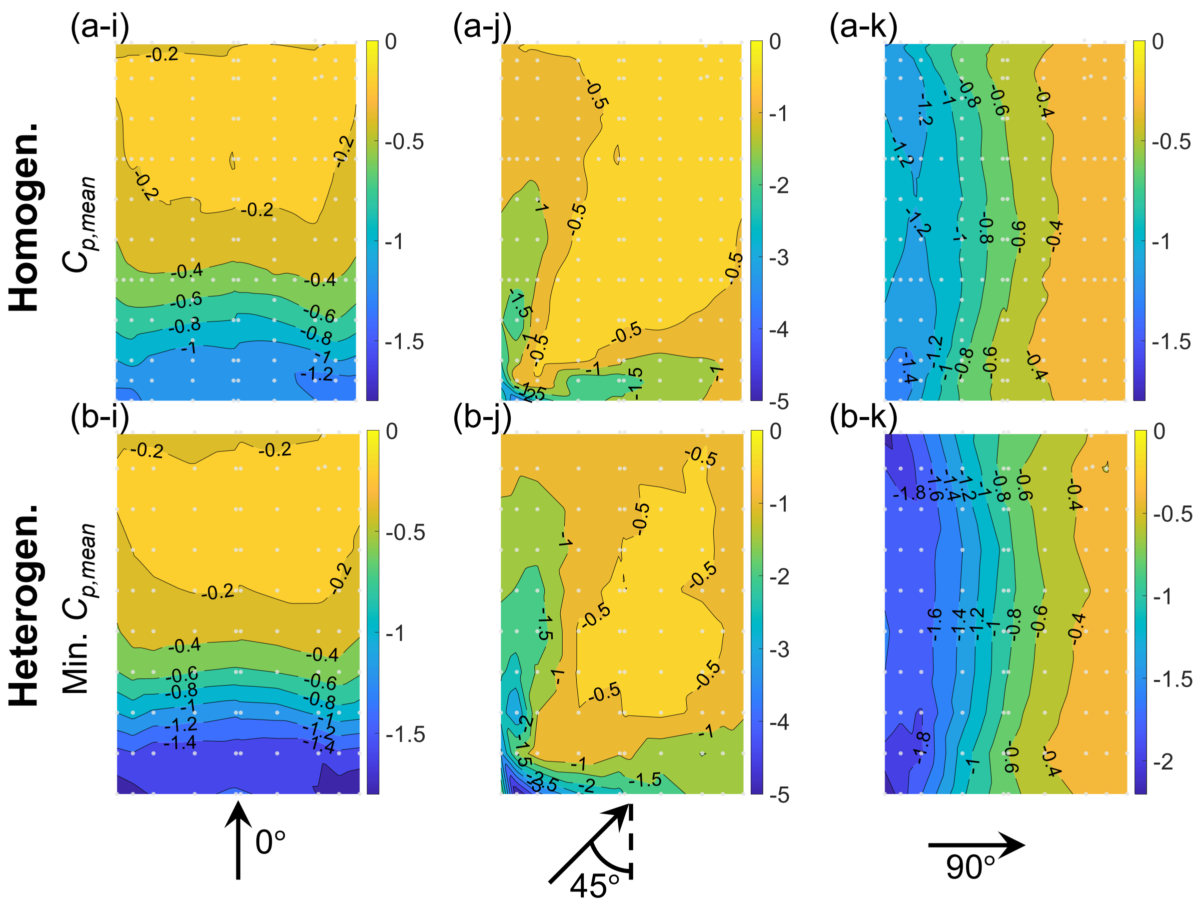

Fig. 12. Comparison of $C_{p,mean}$ on roof: (a) Homogeneous terrain (H = 0.09 m); and (b) Envelop of selected heterogeneous terrains (0.30 m< $z_{0,eff}$ ≤0.34 m); with wind incident angle of (i) 0°; (j) 45°; and (k) 90°.

This file is the final accepted version of the manuscript, published in
https://doi.org/10.1016/j.jobe.2023.108350

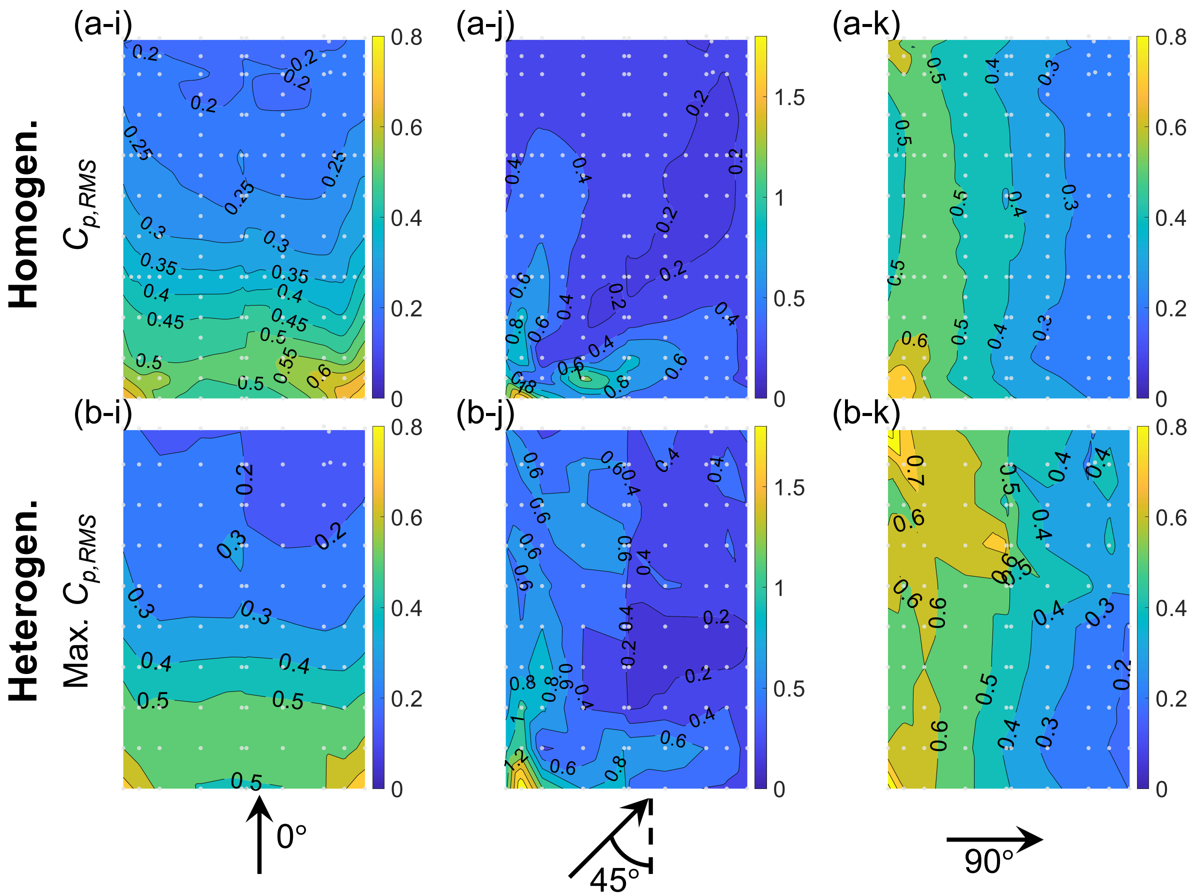

Fig. 13. Comparison of $C_{p,RMS}$ on roof: (a) Homogeneous terrain (H = 0.09 m); and (b) Envelop of selected heterogeneous terrains (0.30 m<$z_{0,eff}$≤0.34 m); with wind incident angles of (i) 0°; (j) 45°; and (k) 90°.

Fig. 14 illustrates the relationship between $I_{u,eave}$ and the peak of statistics: (i) Minimum $C_{p,mean}$ and (j) Maximum $C_{p,RMS}$, on the entire roof at the three wind incident angles: (a) 0°; (b) 45°; and (c) 90°. While the peaks of statistics were predominantly observed at the corner of the leading edge. The overall pressure behavior was similar to that observed in the tap line.

The minimum $C_{p,mean}$ increased continuously as $I_{u,eave}$ increased, with larger suction occurring in heterogeneous terrain compared to homogeneous terrain. This pattern was consistently observed at 0°, 45°, and 90°.

The trend of maximum $C_{p,RMS}$ increasing as $I_{u,eave}$ rises was observed in both homogeneous and heterogeneous terrains. However, heterogeneous terrain did not exhibit a greater magnitude. This pattern was equally observed at 0°, 45°, and 90°.

As depicted in Fig. 14 (b), at a wind incident angle of 45°, significant variability occurs due to the influence of conical vortices [10]. Consequently, minimum $C_{p,mean}$ and maximum $C_{p,RMS}$ of relatively large magnitude were observed compared to 0° or 90°. At this angle, the minimum $C_{p,mean}$ for homogeneous terrain was only about -3.7, while the minimum $C_{p,mean}$ for heterogeneous terrain was observed to reach up to -6, an increase of more than 50%.

464 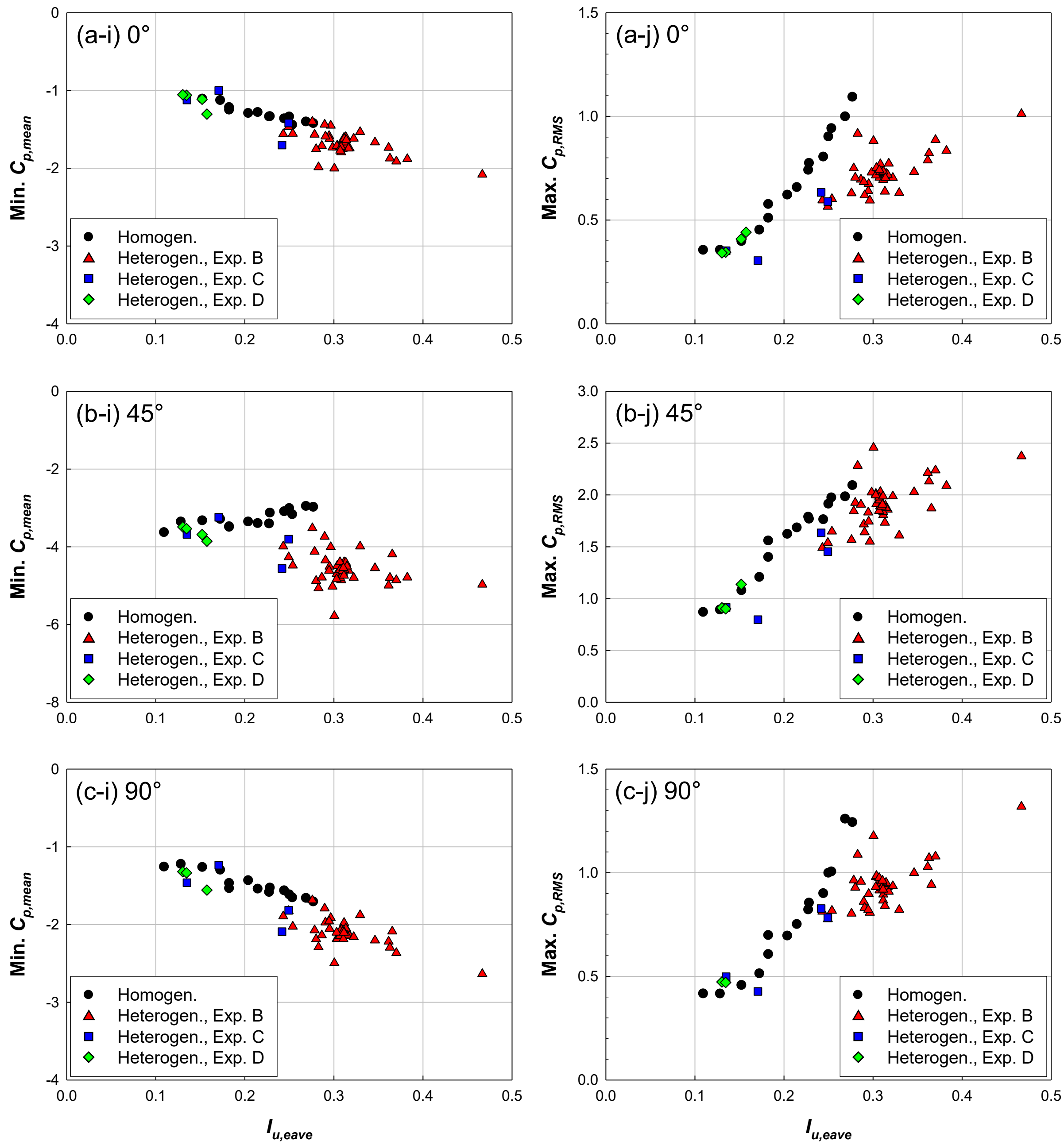

465 Fig. 14. Relationship between $I_{u,eave}$ and the peak statistics on the roof: Wind incident angles of (a) 0°; (b) 45°; and
466 (c) 90°; with (i) Minimum $C_{p,mean}$; and (j) Maximum $C_{p,RMS}$.

467

468

469

This file is the final accepted version of the manuscript, published in
https://doi.org/10.1016/j.jobe.2023.108350

5. Conclusions

This study conducted extensive wind tunnel tests using 50 actual terrain morphologies in the US to investigate the impact of terrain complexity on wind pressure for low-rise buildings. The results were compared with testing on homogeneous terrain to analyze variations in pressure coefficients. The main findings are as follows:

- Complex heterogeneous terrain exhibited stronger turbulence intensity compared to homogeneous terrain, even with similar $z_{0,\text{eff}}$. After calculating $z_{0,\text{eff}}$ using the anemometric method, wind characteristics at sites corresponding to the same exposure were compared. While there was no difference in mean wind speed between homogeneous terrain and complex heterogeneous terrain, turbulence intensity was approximately 35% higher on average in heterogeneous terrain. This disparity in turbulence properties proved to be a crucial factor in explaining the change in $C_{p,mean}$ in heterogeneous terrains.

- The analysis of pressure coefficient statistics along the tap line leading to the windward wall, roof, and leeward wall revealed that the magnitude of statistics increased in both homogeneous terrain and heterogeneous terrain as $z_{0,\text{eff}}$ increased. This phenomenon may occur because increased wind turbulence in cases with higher $z_{0,\text{eff}}$ directly affects the resizing of vortices and oscillations. Also, terrain complexity may increase the magnitude of the peak of $C_{p,mean}$ on the windward wall and the roof 1. Around the typical z_0 of Exposure B (0.3 m), it was observed that the peak of $C_{p,mean}$ on the windward wall and roof 1 increased by approximately 75% and 50% compared to homogeneous terrain, respectively. Conversely, no discernible difference was observed between homogeneous terrain and heterogeneous terrain on roof 2 (downwind region on the roof) and the leeward wall. Thus, in windward wall and roof 1 regions, changes in turbulence properties resulting

This file is the final accepted version of the manuscript, published in
https://doi.org/10.1016/j.jobe.2023.108350

from terrain complexity would have an insignificant impact due to flow reattachment and the wake generated by the structure itself.

- $C_{p,mean}$ is primarily influenced by $I_{u,eave}$. In the windward wall and roof 1 regions, the magnitude of peak $C_{p,mean}$ continuously rose as $I_{u,eave}$ increased. Notably, it was observed that the correlation between $I_{u,eave}$ and $C_{p,mean}$, previously established for $I_{u,eave}$ values below 0.3, also held true for higher $I_{u,eave}$ values exceeding 0.3. However, In the case of $C_{p,RMS}$, the same tendency for the value to increase as $I_{u,eave}$ increased was observed. Unlike $C_{p,mean}$, the phenomenon of magnitude continuously increasing as $I_{u,eave}$ increased was not observed. Therefore, no significant difference in magnitude was observed between homogeneous terrain and complex heterogeneous terrain.
- Examination of the roof contour confirmed that the reattachment length in complex heterogeneous terrain was longer than that in homogeneous terrain. This was attributed to the higher turbulence intensity level in heterogeneous terrain, leading to a reduction in the shear layer's radius of curvature. The trends observed for minimum $C_{p,mean}$ and maximum $C_{p,RMS}$ on the entire roof were similar to those of the tap line.
- For Exposure B, significant terrain complexity could arise due to the wider range of z_0 compared to Exposures C and D, resulting in the highest $I_{u,eave}$. This led to $C_{p,mean}$ with the largest magnitude. Comparison of the minimum $C_{p,mean}$ on the roof when the wind incidence angle was 45° revealed that while it did not exceed -4 in homogeneous terrain, it could reach -6 in complex heterogeneous terrain. Relying on a hasty homogeneous terrain assumption may lead to substantial errors in wind load assessment, emphasizing the need for additional examination of the influence of terrain complexity.

6. Acknowledgments

This material is based upon work supported by the National Science Foundation under Grant No. CMMI-1856205. Any opinions, findings, and conclusions or recommendations expressed in this material are those of the authors and do not necessarily reflect the views of the National Science Foundation.

7. References

[1] A.G. Davenport, Past, present and future of wind engineering, J. Wind. Eng. Ind. Aerod. 90(12-15) (2002) 1371-1380. https://doi.org/10.1016/S0167-6105(02)00383-5.
[2] ASCE, Minimum design loads and associated criteria for buildings and other structures, 7-22, American Society of Civil Engineers, 2022. https://doi.org/10.1061/9780784415788.
[3] K. Wang, T. Stathopoulos, Exposure model for wind loading of buildings, J. Wind. Eng. Ind. Aerod. 95(9-11) (2007) 1511-1525. https://doi.org/10.1016/j.jweia.2007.02.016.
[4] M. Jensen, The model law for phenomena in natural wind, Reprint from Ingenioren (international edition) 2(4) (1958) 121-128.
[5] H. Tieleman, Wind tunnel simulation of wind loading on low-rise structures: a review, J. Wind. Eng. Ind. Aerod. 91(12-15) (2003) 1627-1649. https://doi.org/10.1016/j.jweia.2003.09.021.
[6] C. Grimmond, T.R. Oke, Aerodynamic properties of urban areas derived from analysis of surface form, J. Appl. Meteorol. Climatol. 38(9) (1999) 1262-1292. https://doi.org/10.1175/1520-0450(1999)038%3C1262:APOUAD%3E2.0.CO;2.
[7] J. Wiernga, Representative roughness parameters for homogeneous terrain, Bound. Layer Meteorol. 63(4) (1993) 323-363. https://doi.org/10.1007/BF00705357.
[8] T. Ho, D. Surry, D. Morrish, NIST/TTU cooperative agreement–windstorm mitigation initiative: Wind tunnel experiments on generic low buildings, London, Canada: BLWTSS20–2003, Boundary-Layer Wind Tunnel Laboratory, Univ. of Western Ontario (2003).
[9] T. Ho, D. Surry, A. Davenport, Variability of low building wind loads due to surroundings, J. Wind. Eng. Ind. Aerod. 38(2-3) (1991) 297-310. https://doi.org/10.1016/0167-6105(91)90049-3.
[10] T. Stathopoulos, Wind loads on low-rise buildings: a review of the state of the art, Eng. Struct. 6(2) (1984) 119-135. https://doi.org/10.1016/0141-0296(84)90005-1.
[11] D. Surry, Pressure measurements on the Texas Tech building: wind tunnel measurements and comparisons with full scale, J. Wind. Eng. Ind. Aerod. 38(2-3) (1991) 235-247. https://doi.org/10.1016/0167-6105(91)90044-W.
[12] X. Wang, Q. Li, B. Yan, Full-scale measurements of wind pressures on a low-rise building during typhoons and comparison with wind tunnel test results and aerodynamic database, Journal of Structural Engineering 146(10) (2020) 04020196. https://doi.org/10.1061/(ASCE)ST.1943-541X.0002769.
[13] I. Zisis, T. Stathopoulos, Wind load transfer mechanisms on a low wood building using full-scale load data, J. Wind. Eng. Ind. Aerod. 104 (2012) 65-75. https://doi.org/10.1016/j.jweia.2012.04.003.

[14] P.L. Fernández-Cabán, F.J. Masters, Experiments in a large boundary layer wind tunnel: Upstream terrain effects on surface pressures acting on a low-rise structure, Journal of Structural Engineering 146(8) (2020) 04720002. https://doi.org/10.1061/(ASCE)ST.1943-541X.0002690.
[15] P. Fernández-Cabán, F. Masters, Near surface wind longitudinal velocity positively skews with increasing aerodynamic roughness length, J. Wind. Eng. Ind. Aerod. 169 (2017) 94-105. https://doi.org/10.1016/j.jweia.2017.06.007.
[16] Z. Ding, W. Zhang, D. Zhu, Neural-network based wind pressure prediction for low-rise buildings with genetic algorithm and Bayesian optimization, Eng. Struct. 260 (2022) 114203. https://doi.org/10.1016/j.engstruct.2022.114203.
[17] Y. Huang, G. Ou, J. Fu, H. Zhang, Prediction of mean and RMS wind pressure coefficients for low-rise buildings using deep neural networks, Eng. Struct. 274 (2023) 115149. https://doi.org/10.1016/j.engstruct.2022.115149.
[18] J. Yu, M. Li, T. Stathopoulos, Q. Zhou, X. Yu, Urban exposure upstream fetch and its influence on the formulation of wind load provisions, Build. Environ. 203 (2021) 108072. https://doi.org/10.1016/j.buildenv.2021.108072.
[19] Y.C. Kim, A. Yoshida, Y. Tamura, Characteristics of surface wind pressures on low-rise building located among large group of surrounding buildings, Eng. Struct. 35 (2012) 18-28. https://doi.org/10.1016/j.engstruct.2011.10.024.
[20] L. An, N. Alinejad, S. Kim, S. Jung, Experimental study on wind characteristics and prediction of mean wind profile over complex heterogeneous terrain, Build. Environ. (2023) 110719. https://doi.org/10.1016/j.buildenv.2023.110719.
[21] A.F. Akon, G.A. Kopp, Mean pressure distributions and reattachment lengths for roof-separation bubbles on low-rise buildings, J. Wind. Eng. Ind. Aerod. 155 (2016) 115-125. https://doi.org/10.1016/j.jweia.2016.05.008.
[22] M. Kiya, K. Sasaki, Free-stream turbulence effects on a separation bubble, J. Wind. Eng. Ind. Aerod. 14(1-3) (1983) 375-386.
[23] S.K. Nasrollah Alinejad, Sungmoon Jung, Wind-Tunnel Testing of Low- and Mid-rise Buildings Under Heterogeneous Upwind Terrains, in: DesignSafe-CI (Ed.) 2023. https://doi.org/10.17603/ds2-6hg9-r131.
[24] N. Alinejad, S. Jung, G. Kakareko, P.L. Fernández-Cábán, Wind-Tunnel Reproduction of Nonuniform Terrains Using Local Roughness Zones, Bound. Layer Meteorol. (2023) 1-22. https://doi.org/10.1007/s10546-023-00822-0.
[25] F.J. Masters, Boundary Layer Wind Tunnel, Basic Operations Manual, University of Florida, Gainesville, FL, 2017.
[26] R.A. Catarelli, P.L. Fernández-Cabán, B.M. Phillips, J.A. Bridge, F.J. Masters, K.R. Gurley, D.O. Prevatt, Automation and new capabilities in the university of Florida NHERI Boundary Layer Wind Tunnel, Frontiers in Built Environment 6 (2020) 558151. https://doi.org/10.3389/fbuil.2020.558151.
[27] R. Kargarmoakhar, A.G. Chowdhury, P.A. Irwin, Reynolds number effects on twin box girder long span bridge aerodynamics, Wind & structures 20(2) (2015) 327-347.
[28] Scanivalve, ZOC33 Miniature Pressure Scanner., 2023. http://scanivalve.com/products/pressure-measurement/miniature-analogpressure-scanners/zoc33-miniature-pressure-scanner/. (Accessed April 13rd 2023).
[29] M. Kovaerk, L. Amatucci, K.A. Gillis, F. Potra, J. Ratino, M.L. Levitan, D. Yeo, Calibration of dynamic pressure in a tubing system and optimized design of tube configuration: A numerical

and experimental study, National Institute of Standards and Technology, Gaithersburg, MD, 2018. https://doi.org/10.6028/NIST.TN.1994.

[30] C. Homer, J. Dewitz, L. Yang, S. Jin, P. Danielson, G. Xian, J. Coulston, N. Herold, J. Wickham, K. Megown, Completion of the 2011 National Land Cover Database for the conterminous United States–representing a decade of land cover change information, Photogramm. Eng. Remote Sens. 81(5) (2015) 345-354. https://doi.org/10.14358/PERS.81.5.345.

[31] A.G. Davenport, Rationale for determining design wind velocities, J. Struct. Div. 86(5) (1960) 39-68. https://doi.org/10.1061/JSDEAG.0000521.

[32] T. Vihma, H. Savijärvi, On the effective roughness length for heterogeneous terrain, Q. J. R. Meteorol. 117(498) (1991) 399-407. https://doi.org/10.1002/qj.49711749808.

[33] Y. He, P. Chan, Q. Li, Estimation of roughness length at Hong Kong International Airport via different micrometeorological methods, J. Wind. Eng. Ind. Aerod. 171 (2017) 121-136. https://doi.org/10.1016/j.jweia.2017.09.019.

[34] D. Arthur, S. Vassilvitskii, K-means++ the advantages of careful seeding, Proceedings of the eighteenth annual ACM-SIAM symposium on Discrete algorithms, 2007, pp. 1027-1035.

[35] R. Macdonald, R. Griffiths, D. Hall, An improved method for the estimation of surface roughness of obstacle arrays, Atmos. Environ. 32(11) (1998) 1857-1864. https://doi.org/10.1016/S1352-2310(97)00403-2.

[36] NRC, National building code of Canada, Associate Committee on the National Building Code, National Research Council1990.

[37] BS, Eurocode 1: actions on structures–part1-4: general actions-wind actions; BS EN 1991-1-4: 2005, British Standard Institution, London, British Standard, 2005.

[38] A. Karimpour, N. Kaye, Z. Baratian-Ghorghi, Modeling the neutrally stable atmospheric boundary layer for laboratory scale studies of the built environment, Build. Environ. 49 (2012) 203-211. https://doi.org/10.1016/j.buildenv.2011.09.026.

[39] R. Catarelli, P. Fernández-Cabán, F. Masters, J. Bridge, K. Gurley, C. Matyas, Automated terrain generation for precise atmospheric boundary layer simulation in the wind tunnel, J. Wind. Eng. Ind. Aerod. 207 (2020) 104276. https://doi.org/10.1016/j.jweia.2020.104276.

[40] Y. Uematsu, N. Isyumov, Wind pressures acting on low-rise buildings, J. Wind. Eng. Ind. Aerod. 82(1-3) (1999) 1-25. https://doi.org/10.1016/S0167-6105(99)00036-7.

[41] A.K. Blackadar, H. Tennekes, Asymptotic similarity in neutral barotropic planetary boundary layers, J. Atmos. Sci. 25(6) (1968) 1015-1020. https://doi.org/10.1175/1520-0469(1968)025%3C1015:ASINBP%3E2.0.CO;2.

[42] N.J. Cook, Designers guide to wind loading of building structures. Part 1, (1986).

[43] H. Schlichting, K. Gersten, Boundary-layer theory, springer2016.

[44] P. Welch, The use of fast Fourier transform for the estimation of power spectra: a method based on time averaging over short, modified periodograms, IEEE Transactions on audio and electroacoustics 15(2) (1967) 70-73. 10.1109/TAU.1967.1161901.

[45] ESDU, Characteristics of atmospheric turbulence near the ground, Part I: Definitions and general information, Engineering Sciences Data Unit 74030 (1974).

[46] E. Gavanski, K.R. Gurley, G.A. Kopp, Uncertainties in the estimation of local peak pressures on low-rise buildings by using the Gumbel distribution fitting approach, Journal of Structural Engineering 142(11) (2016) 04016106. https://doi.org/10.1061/(ASCE)ST.1943-541X.0001556.

[47] J. Lieblein, Efficient methods of extreme-value methodology, 1976.

[48] X. Wang, Q. Li, J. Li, Field monitoring and wind tunnel study of wind effects on roof overhang of a low-rise building, Structural Control and Health Monitoring 27(3) (2020) e2484. https://doi.org/10.1002/stc.2484.
[49] T. Ghazal, J. Chen, M. Aboutabikh, H. Aboshosha, S. Elgamal, Flow-conditioning of a subsonic wind tunnel to model boundary layer flows, Wind and structures 30(4) (2020) 339. https://doi.org/10.12989/was.2020.30.4.339.
[50] H. Tieleman, D. Surry, K. Mehta, Full/model-scale comparison of surface pressures on the Texas Tech experimental building, J. Wind. Eng. Ind. Aerod. 61(1) (1996) 1-23. https://doi.org/10.1016/0167-6105(96)00042-6.
[51] Z. Zhao, Wind flow characteristics and their effects on low-rise buildings, Texas Tech University1997.
[52] R. Hillier, N. Cherry, The effects of stream turbulence on separation bubbles, J. Wind. Eng. Ind. Aerod. 8(1-2) (1981) 49-58. https://doi.org/10.1016/0167-6105(81)90007-6.
[53] A.F. Akon, Effects of turbulence on the separating-reattaching flow above surface-mounted, three-dimensional bluff bodies, The University of Western Ontario (Canada), 2017.
[54] H. Okada, Y.-C. Ha, Comparison of wind tunnel and full-scale pressure measurement tests on the Texas Texh Building, J. Wind. Eng. Ind. Aerod. 43(1-3) (1992) 1601-1612. https://doi.org/10.1016/0167-6105(92)90375-K.
[55] P.L. Fernández-Cabán, F.J. Masters, Effects of freestream turbulence on the pressure acting on a low-rise building roof in the separated flow region, Frontiers in Built Environment 4 (2018) 17. Volume 4 - 2018 | https://doi.org/10.3389/fbuil.2018.00017.
[56] I.S. Gartshore, The effects of free stream turbulence on the drag of rectangular two-dimensional prisms, University of Western Ontario, Faculty of Engineering Science, 1973.